Subsalt imaging improvement possibilities through a combination of FWI and reflection FWI

Chao Peng[1], Minshen Wang[1], Nicolas Chazalnoel[1], and Adriano Gomes[1]

Abstract

Despite continuous improvements in seismic acquisition and processing technology, imaging under salt remains challenging, specifically because of the difficulty in updating complex salt geometries and subsalt velocity. Synthetic studies show that when certain conditions are met, full-waveform inversion (FWI) can recover very complex velocity models, including the geometry of the salt and the subsalt velocity. Unfortunately, currently available seismic field data fall short of meeting the requirements needed to replicate what can be achieved on synthetic data. We first use a wide-azimuth data set from the Mexican side of the Gulf of Mexico (GOM) to show how FWI can improve imaging in the subsalt. In addition to utilizing the diving-wave energy to derive a reliable model in the shallow sediment overburden, we use reflection FWI (RFWI) to update the velocity model in the deep area. RFWI utilizes the low-wavenumber components of the FWI gradient associated with waves reflected in the model, which makes it possible to circumvent the well-known penetration-depth limitation of FWI and the shortcomings of traditional tomography-based methods. This is achieved by alternately using the high-wavenumber and low-wavenumber components of the FWI gradient to update density and velocity models, respectively. We then use an ultralong-offset, full-azimuth data set from the U.S. side of the GOM to show that, with more suitable data, FWI and RFWI can be combined to recover the velocity in and around complex salt bodies, providing significant uplift to subsalt images.

Introduction

Full-waveform inversion (FWI) (Tarantola, 1984) is now recognized as the method of choice to provide accurate high-resolution velocity for the shallower part of velocity models (Sirgue and Pratt, 2004). While impressive results have been achieved using FWI for updating the salt and subsalt of the velocity model on synthetic data sets, the same level of benefit has not yet been achieved on a field data set. The gap between what FWI achieves on synthetic data and what FWI achieves on field data is likely due to imperfect seismic data. Specifically, conventional FWI relies on diving waves, the penetration of which is limited to the shallow part of the model due to the limited offsets of typical acquisitions. Furthermore, good-quality low-frequency signal is also required to drive the inversion in the right direction when the initial model is not close enough to the true model, but good low-frequency signal is often lacking in seismic field data.

Recently, new subsurface imaging developments have been proposed to close the gap between FWI requirements and the data sets available, either by extending the minimum-usable low frequency in the seismic data (Dellinger et al., 2016) or by treating salt bodies differently in the FWI objective function (Esser et al., 2015; Datta et al., 2016; Kadu et al., 2016). However, these approaches have yet to make the transition to consistent real-data applications. Therefore, the most common method for updating salt geometry remains to manually pick the different salt boundaries through different migration steps. This method requires good geologic knowledge, can be quite time-intensive and challenging, and often fails to recover the full complexity of the salt geometry (Dellinger et al., 2017). For the subsalt, reverse time migration (RTM) angle gathers (Li et al., 2011; Xu et al., 2011) or surface-offset gathers (SOGs) (Yang et al., 2015) are used to update the velocity tomographically. A drawback of these approaches is their reliance on the quality of the gathers under the salt, making it difficult to estimate the dip and residual curvature. Another drawback is their dependence on ray-based tomography, which is often unstable around salt, to update the velocity.

To circumvent the diving-wave penetration limitation of FWI, reflection-based waveform inversions have been proposed in the past (Chavent et al., 1994; Xu et al., 2012) and have recently regained traction in the industry. As shown by Mora (1989), reflection data produce two different components in the FWI gradient: the high-wavenumber component, also known as the migration term, and the low-wavenumber component, also known as the tomographic term or "rabbit ears." This tomographic term is generated along the reflection wavepath; therefore, it contains significant information about the kinematics of the velocity model, including areas beyond the reach of diving waves. In an attempt to exploit this property of the tomographic term and update the deeper part of the velocity model, we follow the reflection FWI (RFWI) method presented by Gomes and Chazalnoel (2017), which alternately uses the high-wavenumber and low-wavenumber components of the FWI gradient to update density and velocity models, respectively.

What FWI can do on synthetic data

We first use a synthetic example to show the capability of FWI with the right data. In this example, we generated synthetic data through acoustic modeling using the BP 2004 model (Billette and Brandsberg-Dahl, 2005). Figure 1a shows a portion of the velocity model that has very complex salt geometry. The initial model provided to FWI is a heavily smoothed sediment model without any salt, as shown in Figure 1b. Figure 1c shows the inversion output from FWI, which is very close to the true model except for the sharp boundary at the sediment and salt interface. In this case, FWI does an almost perfect job recovering the complex model, including the salt geometry and subsalt velocity, starting from a model that is far removed from the true model.

However, to achieve this, the synthetic data we generated for the inversion have 30 km ultralong offsets and contain low-frequency signal down to 0.5 Hz. In reality, these requirements are hard to meet, especially the low-frequency aspect. For field data,

[1]CGG.

https://doi.org/10.1190/tle37010052.1.

the lowest usable frequency normally starts from 4 Hz for a marine environment; though in some acquisitions the limit can be brought down to 2 to 2.5 Hz (Mandroux et al., 2013; Dellinger, 2016). Figures 2b and 2c show the inversion results with data that have lowest usable signal from 2 and 4 Hz, respectively. Even with 30 km ultralong offset, the inversion fails to recover the true model. To a certain extent, the lack of low frequencies could be overcome if a better starting model was achieved with traditional methods so that FWI is not compromised by cycle skipping. Figure 3a shows another initial model with incorrect salt interpretation at the rugose top of salt (TOS) and overhang areas. Unlike the inversion from the sediment model, FWI successfully corrects these misinterpretations with 2 Hz and 30 km offset data, as shown in Figure 3b. But the offset limitation, which dictates the penetration of the diving waves, remains an obstacle for conventional FWI (Sirgue and Pratt, 2004). Figure 3c shows the FWI result with 4 Hz and 9 km offset data, which is typical for wide-azimuth (WAZ) acquisitions. In this case, FWI fails to recover the true model, especially for the deeper part, due to the lack of diving-wave penetration.

RFWI

To reduce the need for long-offset acquisitions and reliance on the refraction energy in the data, RFWI (Xu et al., 2012) uses the low-wavenumber component of the FWI gradient of reflection data to update deeper parts of the model. As shown in Figure 4, the FWI gradient is formed by three main components. While FWI normally relies on the transmitted wave term (Figure 4a), RFWI tries to make use of the reflected wave terms (Figures 4b and 4c), which are able to penetrate deeper into the model. The high-wavenumber component (Figure 4b), or migration term, is generated by crosscorrelation of wavefields traveling

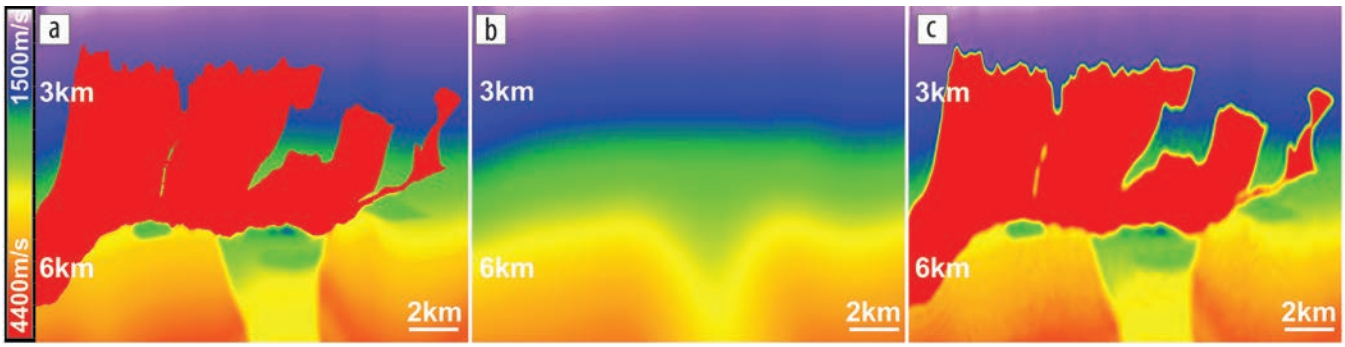

Figure 1. (a) A portion of the BP 2004 velocity model. (b) Heavily smoothed sediment model. (c) FWI inverted model with frequency starting from 0.5 Hz.

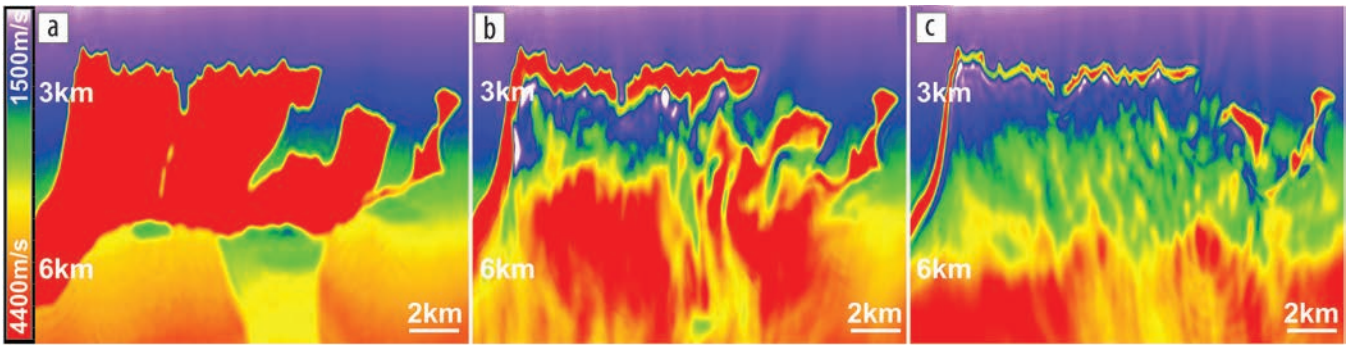

Figure 2. (a) FWI inversion starts from 0.5 Hz. (b) FWI inversion starts from 2 Hz. (c) FWI inversion starts from 4 Hz.

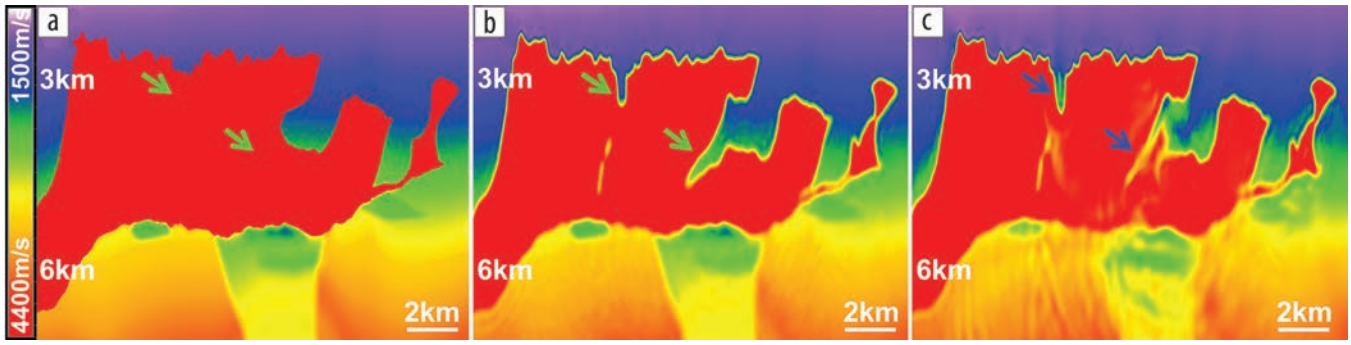

Figure 3. (a) Perturbed BP 2004 model as initial model for FWI with misinterpretation at TOS and overhang area, indicated by the green arrows. (b) FWI inverted model with 2 Hz and 30 km offset data. The green arrows indicate the inversion is successful at resolving the two misinterpretations in the initial model. (c) FWI inverted model with 4 Hz and 9 km offset data. The blue arrows indicate that the inversion fails to resolve the two misinterpretations in the initial model.

in opposite directions, and its wavenumber content normally has limited impact on the kinematics of the model. The low-wavenumber component, or tomographic term, is generated along the reflection wavepath by crosscorrelation of incident and reflected/scattered wavefields traveling in the same direction (Mora, 1989); therefore, it contains significant information about the kinematics of the velocity model and is the base for the RFWI velocity update. Separation of the tomographic term from the migration term can then be achieved based on the propagation directions of the source and receiver wavefields (Liu et al., 2011; Tang et al., 2013; Irabor and Warner, 2016). In our RFWI implementation, the high-wavenumber and low-wavenumber terms are used alternately to update density and velocity models, respectively. The high-wavenumber density update introduces the deep reflectors that will generate the back-scattered energy needed for the next iteration of low-wavenumber velocity updates. In this latter iteration, since the reflector depths are self-derived from the current velocity model, the timing of the synthetic data matches the real data in a certain offset range (typically near offsets, which dominate the stack). RFWI will then derive the velocity update from the timing mismatch at different offsets. Because it relies on reflection data, RFWI can produce updates to the velocity model along the reflection wavepaths, beyond the reach of diving waves. Despite the limited angle coverage of deep reflectors (Gomes and Chazalnoel, 2017), RFWI is still able to improve the traveltimes that have significant impact on the migrated images. Once the kinematics of the model are improved, the migration term can be used later in a conventional FWI manner, to recover the high wavenumbers that cannot be retrieved by RFWI (Irabor and Warner, 2016).

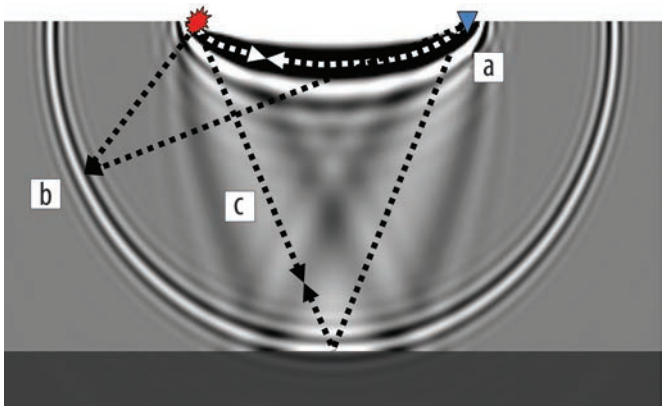

Figure 4. Single-trace FWI gradient on a medium with a single reflector. Component (a) is generated by transmitted waves, while components (b) and (c) are generated by reflected waves.

RFWI on WAZ data

We use WAZ field data to illustrate what RFWI can do for subsalt imaging. The area is located in the western Gulf of Mexico (GOM) on the Mexican side of the prolific Perdido fold belt. The water depth ranges from 1500 to 3500 m. We start with a velocity model that underwent several iterations of tomography and FWI updates for the overburden, typical model building for the salt geometry, and a subsalt velocity update using well information and scans. Data preprocessing steps for RFWI include denoise, source and receiver deghosting, designature, and 3D surface-related multiple elimination. The penetration depth for diving-wave energy is no more than 4 km, as the maximum offset is 8.1 km along the cable. Because the subsalt targets are located at a depth of about 8 to 10 km, the benefit from diving-wave energy is limited in this case. We first focus on an area where the starting model was able to update the overburden well but failed to properly update the shale velocity at the bottom of a minibasin because of the lack of reflectivity inside the shale and the shale depth. Sediment flood RTM shows the imaged rugose TOS below the shale body with the starting model (Figure 5a). RFWI was applied from 4 to 7 Hz following the same workflow as presented by Chazalnoel et al. (2017). High-wavenumber components of the FWI gradient were used to update the density down to TOS, which drives the low-wavenumber velocity update above it. Figure 5b shows the sediment flood RTM image after the RFWI update. We see improvements in the imaging of the TOS: overmigrated

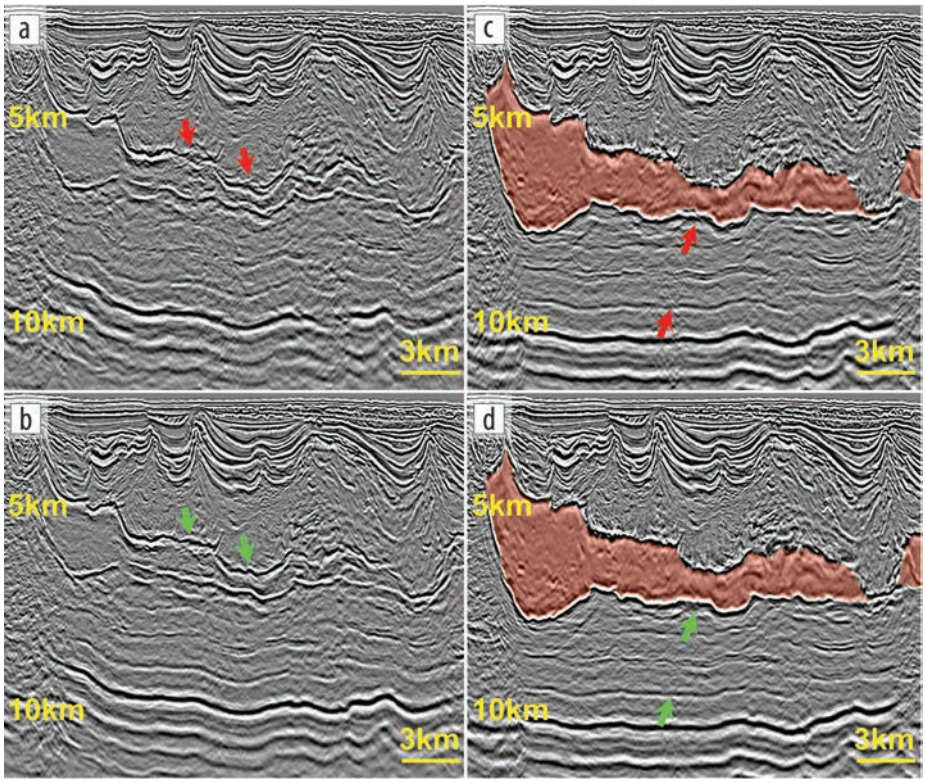

Figure 5. Sediment flood RTM shows TOS (a) before and (b) after suprasalt RFWI. (c) Salt body (red) RTM image before the update. (d) Suprasalt RFWI and reinterpretation improved the focusing of the BOS and continuity of subsalt. The red arrows point to the poorly focused TOS, BOS, and subsalt events before RFWI, while the green arrows point to the improved images after RFWI.

swings on the peak event are now more coherent. The TOS and base of salt (BOS) were reinterpreted, respectively, based on the sediment and salt floods using RFWI velocity. Improved images of both the BOS and subsalt show the impact of the suprasalt velocity accuracy on salt interpretation (Figures 5c and 5d).

Following the shallow sediment update and salt geometry refinement, we applied RFWI allowing an update of the sediment inclusion velocity inside the salt and the subsalt velocity. In Figure 6, we show an example where a thick salt body was barely penetrated by diving waves. The complexity of the deep folds and the velocity uncertainty of the intrasalt inclusion make it difficult for conventional velocity update methods to generate a viable solution. RFWI is able to improve both the velocity model and the corresponding image down to a depth of more than 10 km. This can be seen clearly from the improved continuity of the deep Wilcox and Cretaceous events (Figures 6a and 6b) in the center of the image. Figure 7a shows the potential vertical aspect of the velocity perturbation from RFWI (Gomes and Chazalnoel, 2017) and also the limited update on the far left side of the image, due to the lack of the deep reflections required for RFWI to work. RTM SOGs show that both event coherency and flatness are improved, confirming that the update, although not perfect, provides a clear uplift (Figures 7b and 7c). Interestingly, the curvatures of deep events in the SOGs before the RFWI update varied rapidly along the line (green and red markers in Figure 7b), making it difficult for conventional ray-based tomography to update; after the RFWI update, the curvatures in the SOGs are almost flat (green and red markers in Figure 7c), suggesting the overburden kinematic error is greatly reduced after RFWI.

Can we do better?

The previous example shows how RFWI can help to reduce kinematic errors for subsalt targets with WAZ acquisition, resulting in a more focused image as well as flatter gathers. RFWI has clearly helped but still falls short of the FWI improvement in the synthetic example shown in Figure 1c. If the mismatch is due to imperfect data, is it possible to narrow this gap with better-designed acquisitions?

In recent years, we have seen a number of new acquisition designs in the GOM aiming to resolve the complex imaging problems in the subsalt (Moldoveanu and Kapoor, 2009; Mandroux et al., 2013; Long et al., 2014). These acquisition designs have full-azimuth (FAZ) coverage and ultralong offsets that are greater than 14 km. Among these, the design with staggered vessels is a good candidate for FWI, as it has offsets up to 18 km, with reliable low-frequency data down to at least 2.5 Hz, thanks to the 50 m tow depth.

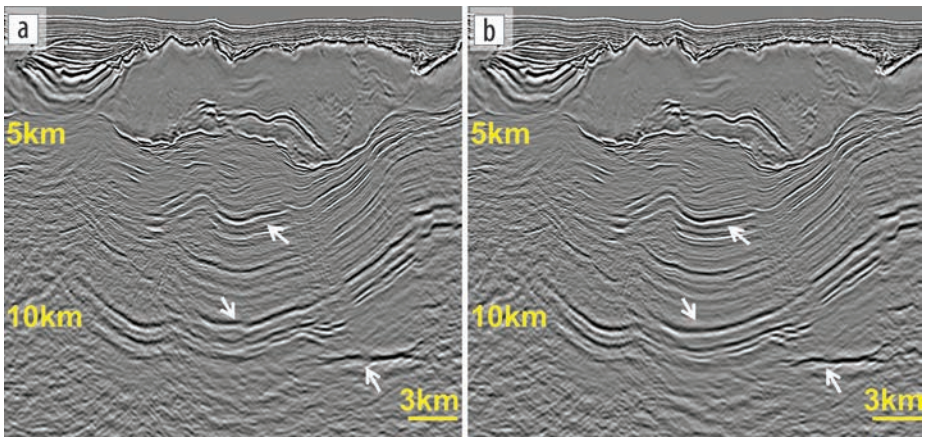

Figure 6. Depth section of RTM stack for: (a) initial model and (b) RFWI updated model. White arrows indicate image improvements at the Wilcox and Cretaceous events.

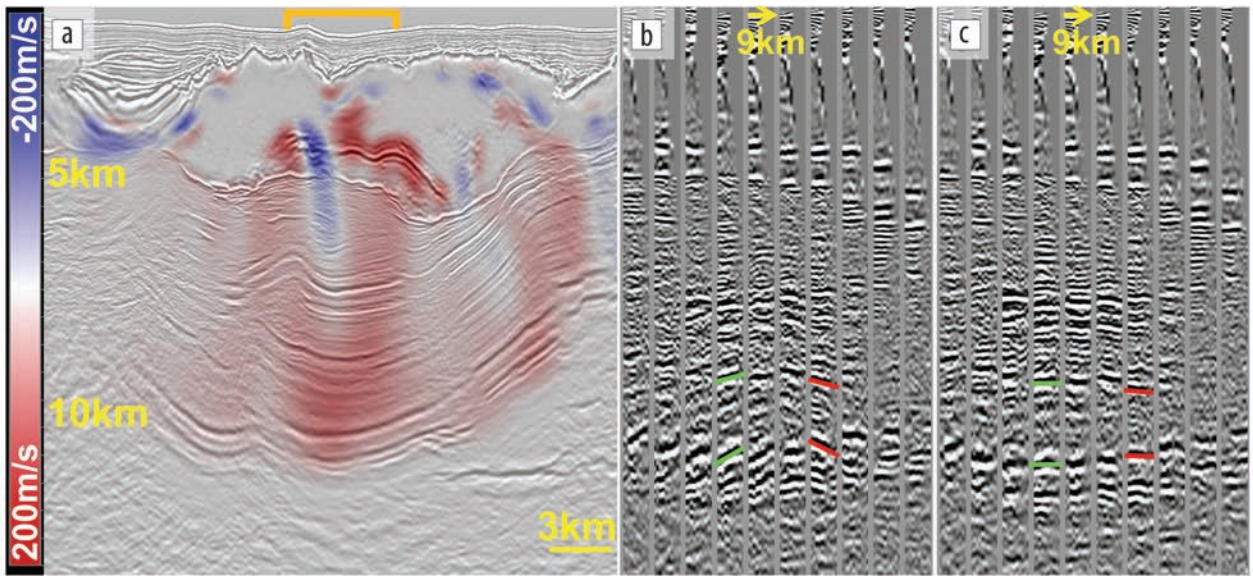

Figure 7. For the same line as Figure 6: (a) velocity-model perturbation from RFWI overlaid on RTM stack with updated model. The orange bracket shows the location of SOGs in (b) and (c). (b) RTM SOGs from initial model and (c) RTM SOGs from RFWI updated model. Green and red markers indicate the picked curvatures on the SOGs before and after the RFWI update.

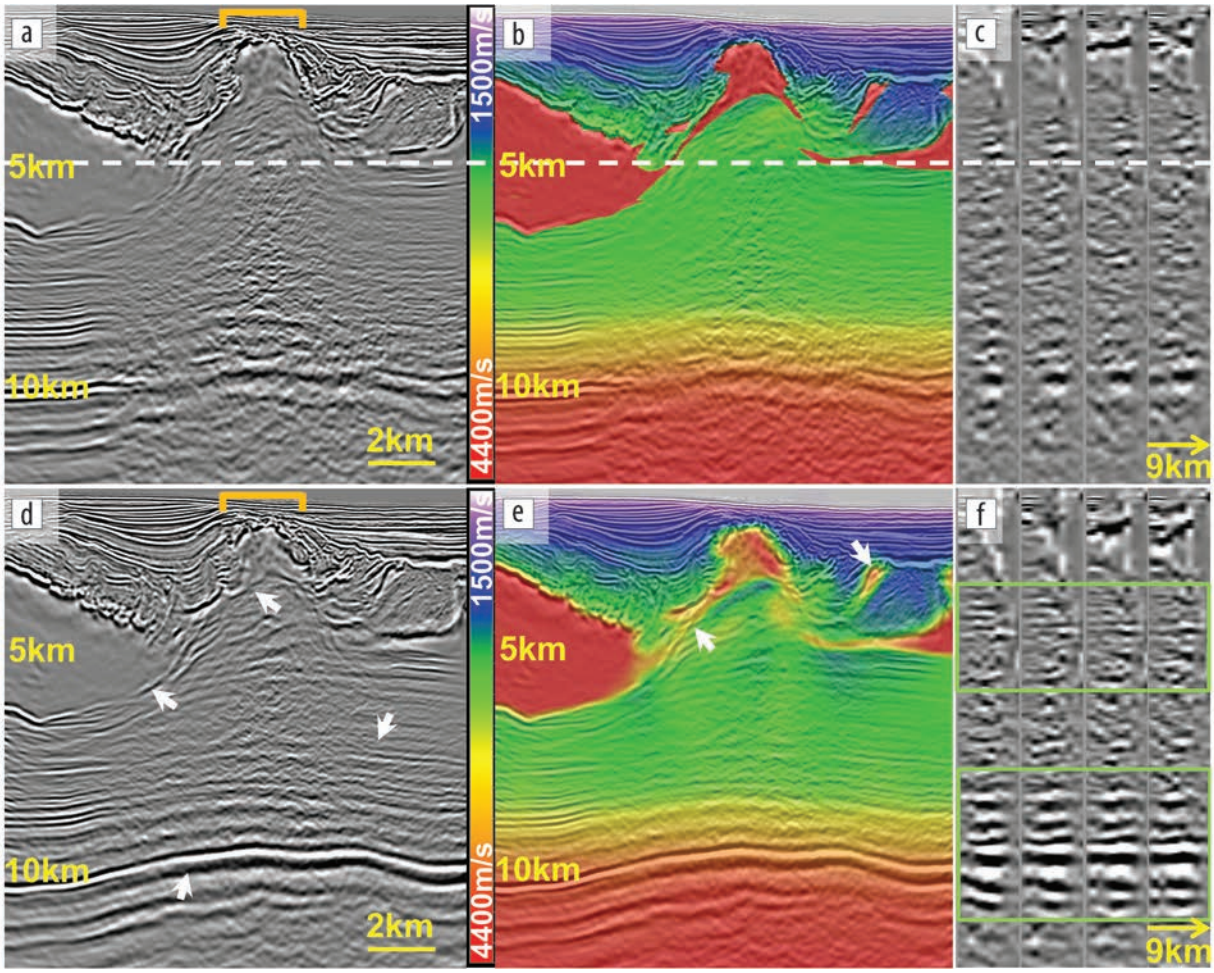

Figure 8. Depth section in the area of study before the FWI update: (a) RTM stack, (b) stack with velocity model overlaid, and (c) RTM SOGs. The dashed white line indicates the approximate penetration depth for diving-wave energy with 18 km maximum offsets. The orange bracket shows the location of the SOGs. Depth section after FWI+RFWI update is shown below: (d) RTM stack, (e) stack with velocity overlaid, and (f) RTM SOGs. The white arrows indicate places where the velocity model and stack image are improved. The green boxes indicate the improvements in RTM SOGs around the center of the image.

We use a data set from this FAZ staggered-vessel acquisition to illustrate what FWI can do with more suitable data. The area of study is in the South Keathley Canyon in the GOM, where salt diapirs appear close to the water bottom. Figure 8a shows a cross section of an image after conventional top-down velocity-model building, while Figure 8b shows the corresponding velocity model overlaid with seismic. The subsalt image is already good at the far left side of the image in Figure 8a. However, because of the complex salt geometry and uncertainty in the sediment model around it, the subsalt image is poor from the middle to the right. In this work, we smooth the velocity model around the salt and first apply diving-wave FWI down to about a 5 km depth, which is the approximate penetration depth for this acquisition design with maximum offset up to 18 km. The FWI inversion is run from 2.5 to 7 Hz, with the aim of correcting the velocity around the shallow salt body. After that, RFWI is run from 3.5 to 7 Hz to fill the remaining gap from the diving-wave penetration depth down to the subsalt events. Figures 8d and 8e show the image after RFWI, without and with the velocity model overlaid. Most of the subsalt reflectors are focused after this FWI/RFWI workflow, which requires minimal manual intervention. The improvement in subsalt event focusing ranges from near to far offsets, as can be seen on the RTM SOGs shown in Figures 8c and 8f. Notice that the salt shape has not been changed dramatically, while details have been added to the model in and around the salt, helping the focusing of the subsalt. This level of detail could not be achieved with the conventional human-intensive salt interpretation but is recovered by the combined application of FWI and RFWI.

Conclusions

As demonstrated on synthetic data, FWI is a method that has the potential to recover very complex models with the right data. However, in reality, we often need to deal with imperfect acquisition designs that compromise FWI's achievable benefits. With commonly used WAZ data in the GOM, we have shown that RFWI can correct some of the kinematic errors at subsalt level beyond diving-wave penetration and with data of limited offset range.

We have also demonstrated that with much longer offsets and good low-frequency content, FWI can help the salt inversion on field data as well and can potentially help simplify the labor-intensive salt-model building. More importantly, when combined with RFWI to benefit from kinematic information contained in the deep

reflections, FWI can produce significant subsalt image uplift, which is hard to achieve with conventional methods.

The field data acquisition designs used in the examples are still far removed from the ideal one used in our synthetic tests, which suggests that an even greater improvement can be expected if better data are provided. Ocean-bottom-node (OBN) acquisitions, for instance, often offer more reliable low-frequency information due to the lack of receiver-side ghost and minimal swell noise contamination, combined with ultralong offsets greater than 20 km. These advantages make OBN data an ideal choice for FWI since it can penetrate to most of the target levels of interest with high fidelity of low-frequency signal to ensure reliable updates even for salt within diving-wave penetration. TLE

Acknowledgments

The authors thank CGG Multi-Client & New Ventures and the Mexican National Hydrocarbons Commission for granting permission to present the data sets. The authors thank Tony Huang for his thoughtful discussions and Jason Xu for his help on some of the real-data examples.

Corresponding author: chao.peng@cgg.com

References

Billette, F. J., and S. Brandsberg-Dahl, 2005, The 2004 BP velocity benchmark: 67th Conference and Exhibition, EAGE, Extended Abstracts, B035.

Chavent, G., F. Clément, and S. Gómez, 1994, Automatic determination of velocities via migration-based traveltime waveform inversion: A synthetic data example: 64th Annual International Meeting, SEG, Expanded Abstracts, 1179–1182, https://doi.org/10.1190/1.1822731.

Chazalnoel, N., A. Gomes, W. Zhao, and B. Wray, 2017, Revealing shallow and deep complex geological features with FWI — Lessons learned: 79th Conference and Exhibition, EAGE, Extended Abstracts, https://doi.org/10.3997/2214-4609.201701158.

Datta, D., M. Sen, F. Liu, and S. Morton, 2016, Salt model building by shape-based parameterization and global FWI: 86th Annual International Meeting, SEG, Expanded Abstracts, 1069–1073, https://doi.org/10.1190/segam2016-13867592.1.

Dellinger, J., 2016, Challenges to extending the usable seismic bandwidth at the seafloor in the deepwater Gulf of Mexico: 86th Annual International Meeting, SEG, Expanded Abstracts, 66–70, https://doi.org/10.1190/segam2016-13762860.1.

Dellinger, J., A. Ross, D. Meaux, A. Brenders, G. Gesoff, J. Etgen, J. Naranjo, G. Openshaw, and M. Harper, 2016, Wolfspar®, an "FWI-friendly" ultralow-frequency marine seismic source: 86th Annual International Meeting, SEG, Expanded Abstracts, 4891–4895, https://doi.org/10.1190/segam2016-13762702.1.

Dellinger, J., A. Brenders, J. R. Sandschaper, C. Regone, J. Etgen, I. Ahmed, and K. J. Lee, 2017, The Garden Banks model experience: The Leading Edge, **36**, no. 2, 151–158, https://doi.org/10.1190/tle36020151.1.

Esser, E., L. Guasch, T. van Leeuwen, A. Arakvin, and F. Herrmann, 2015, Automatic salt delineation — Wavefield reconstruction inversion with convex constraints: 85th Annual International Meeting, SEG, Expanded Abstracts, 1337–1343, https://doi.org/10.1190/segam2015-5877995.1.

Gomes, A., and N. Chazalnoel, 2017, Extending the reach of full-waveform inversion with reflection data: Potential and challenges: 79th Conference and Exhibition, EAGE, Extended Abstracts, WS09 B03, https://doi.org/10.3997/2214-4609.201701714.

Irabor, K., and M. Warner, 2016, Reflection FWI: 86th Annual International Meeting, SEG, Expanded Abstracts, 1136–1140, https://doi.org/10.1190/segam2016-13944219.1.

Kadu, A., T. van Leeuwen, and W. Mulder, 2016, A parametric level-set approach for seismic full-waveform inversion: 86th Annual International Meeting, SEG, Expanded Abstracts, 1146–1150, https://doi.org/10.1190/segam2016-13870276.1.

Li, Z., S. Ji, B. Bai, Q. Wu, and W. Han, 2011, Dirty salt tomography using RTM 3D angle gathers: 81st Annual International Meeting, SEG, Expanded Abstracts, 4020–4024, https://doi.org/10.1190/1.3628046.

Liu, F., G. Zhang, S. Morton, and J. Leveille, 2011, An effective imaging condition for reverse-time migration using wavefield decomposition: Geophysics, **76**, no. 1, S29–S39, https://doi.org/10.1190/1.3533914.

Long, A., S. Campbell, S. Fishburn, S. Brandsberg-Dahl, N. Chemingui, and V. Dirks, 2014, No-compromise marine seismic: A full-azimuth survey design for total-wavefield velocity model building and imaging in the deep-water Gulf of Mexico. 84th Annual International Meeting, SEG, Expanded Abstracts, 52–56, https://doi.org/10.1190/segam2014-1022.1.

Mandroux, F., C. Ting, B. Montgomery, and A. Lenart, 2013, Staggered marine acquisition design for complex imaging: 83rd Annual International Meeting, SEG, Expanded Abstracts, 26–30, https://doi.org/10.1190/segam2013-0354.1.

Moldoveanu, N., and J. Kapoor, 2009, What is the next step after WAZ for exploration in the Gulf of Mexico?: 79th Annual International Meeting, SEG, Expanded Abstracts, 41–45, https://doi.org/10.1190/1.3255750.

Mora, P., 1989, Inversion = migration + tomography: Geophysics, **54**, no. 12, 1575–1586, https://doi.org/10.1190/1.1442625.

Sirgue, L., and R. G. Pratt, 2004, Efficient waveform inversion and imaging: A strategy for selecting temporal frequencies: Geophysics, **69**, no. 1, 231–248, https://doi.org/10.1190/1.1649391.

Tang, Y., S. Lee, A. Baumstein, and D. Hinkley, 2013, Tomographically enhanced full wavefield inversion: 83rd Annual International Meeting, SEG, Expanded Abstracts, 1037–1041, https://doi.org/10.1190/segam2013-1145.1.

Tarantola, A., 1984, Inversion of seismic reflection data in the acoustic approximation: Geophysics, **49**, no. 8, 1259–1266, https://doi.org/10.1190/1.1441754.

Xu, S., Y. Zhang, and B. Tang, 2011, 3D angle gathers from reverse time migration: Geophysics, **76**, no. 2, S77–S92, https://doi.org/10.1190/1.3536527.

Xu, S., D. Wang, F. Chen, Y. Zhang, and G. Lambaré, 2012, Full waveform inversion for reflected seismic data: 74th Conference and Exhibition, EAGE, Extended Abstracts, https://doi.org/10.3997/2214-4609.20148725.

Yang, Z., S. Huang, and R. Yan, 2015, Improved subsalt tomography using RTM surface offset gathers: 85th Annual International Meeting, SEG, Expanded Abstracts, 5254–5258, https://doi.org/10.1190/segam2015-5848366.1.